Finite element analysis of nanowire indentation on a flat substrate

Davood Askari[a] and Gang Feng[b]
Department of Mechanical Engineering, Villanova University, Villanova, Pennsylvania 19085

(Received 28 June 2011; accepted 17 October 2011)

Nanowires have attracted tremendous research interests due to their potential applications. Their mechanical properties are critical for the reliability and durability of the nanowire-based devices. Compared to many other characterization techniques, the lateral probing of a nanowire using nanoindentation has the advantage of relatively simple sample preparation. However, the data analysis is difficult due to the complex contact mechanics. In all previous studies, some questionable approximations have been made to proceed with data analysis. In this study, a quantitative physical picture of nanowire lateral probing is proposed, which we believe is the first time in the literature. Three-dimensional finite element analysis (FEA) is performed and compared to a double-contact analytical model in which the two contacts, namely contact 1 (indenter/nanowire) and contact 2 (nanowire/substrate), are considered. Both the FEA and analytical models are for a specific case: an elastic spherical indention of a GaN nanowire on a Si substrate. We find that contact 1 cannot be well approximated by a Hertzian elliptical contact as assumed in many studies. We also find a large contact deformation at contact 2, which has been ignored in almost all previous studies. Finally, the adhesion condition and nanowire-receding at contact 2 are found to have insignificant effects on the data analysis.

I. INTRODUCTION

Nanowires and nanotubes have wide range of potential applications, such as chemical and optical sensors,[1,2] resonators and force sensors,[3,4] high-resolution scanning probe microscope (SPM) tips,[5] and reinforcements for nanocomposites.[6,7] To design the devices composed of these nanomaterials, it is essential to know their behavior and properties, e.g., mechanical properties for the applications of force sensors, SPM tips, and nanocomposites. Mechanical characterization at such small scales is very challenging.

Nanoindenter and atomic force microscope have been successfully used to laterally indent nanowires and nanotubes,[8–18] whereas the associated rigorous analytical solution is not available due to the complex contact mechanics.[9] Consequently, approximations were made in these previous studies[8–18] to proceed with indentation data analysis. However, some of the approximations may be problematic: (i) treating the nanomaterial as half-space (using the Oliver–Pharr method[19] for data analysis),[10,14,15] (ii) neglecting the contact deformation between the nanomaterial and substrate,[11,16] and (iii) neglecting the possibility of receding (the ends of the nanomaterial being separated from the substrate).[8,10–18] To take account of the aforementioned effects, Feng et al. have proposed a double-contact (two contacts in series) model[9]: contact 1 (indenter/nanowire) is approximated by a Hertzian elliptical contact of sphere/cylinder, and, contact 2 (nanowire/substrate) is approximated by a receding contact of cylinder/half-space. The Hertzian elliptical contact has a closed-form solution.[20] Although the receding contact of cylinder/half-space does not have a rigorous analytical solution, a mechanism-based analytical approximation was empirically derived.[9] However, to our best knowledge, all previous analytical models and data analysis[8–18] on nanowire lateral probing have not been quantitatively compared to numerical models, e.g., finite element analysis (FEA).

In this article, a quantitative physical picture, first time in the literature, is proposed to model the lateral probing of a nanowire, which is used to analyze a three-dimensional (3D) FEA, and the results are compared with that based on the double-contact model.[9]

II. FEA MODELING

As shown in Fig. 1(a), a 3D FEA model is developed using ANSYS 11 for lateral probing of a GaN nanowire on a Si substrate. Again, to our best knowledge, none of previous studies[8–18] have quantitatively compared the analytical or experimental results with the FEA results. Since purely elastic contact modeling would already provide significant physical insights, and moreover all previous analytical models[8,10–18] for nanowire lateral

[a]Present address: Department of Engineering, The University of Texas at Brownsville and Texas Southmost College, 80 Fort Brown, Brownsville, Texas 78520
[b]Address all correspondence to this author.
e-mail: gang.feng@villanova.edu
DOI: 10.1557/jmr.2011.420

 © Materials Research Society 2011

https://doi.org/10.1557/jmr.2011.420 Published online by Cambridge University Press

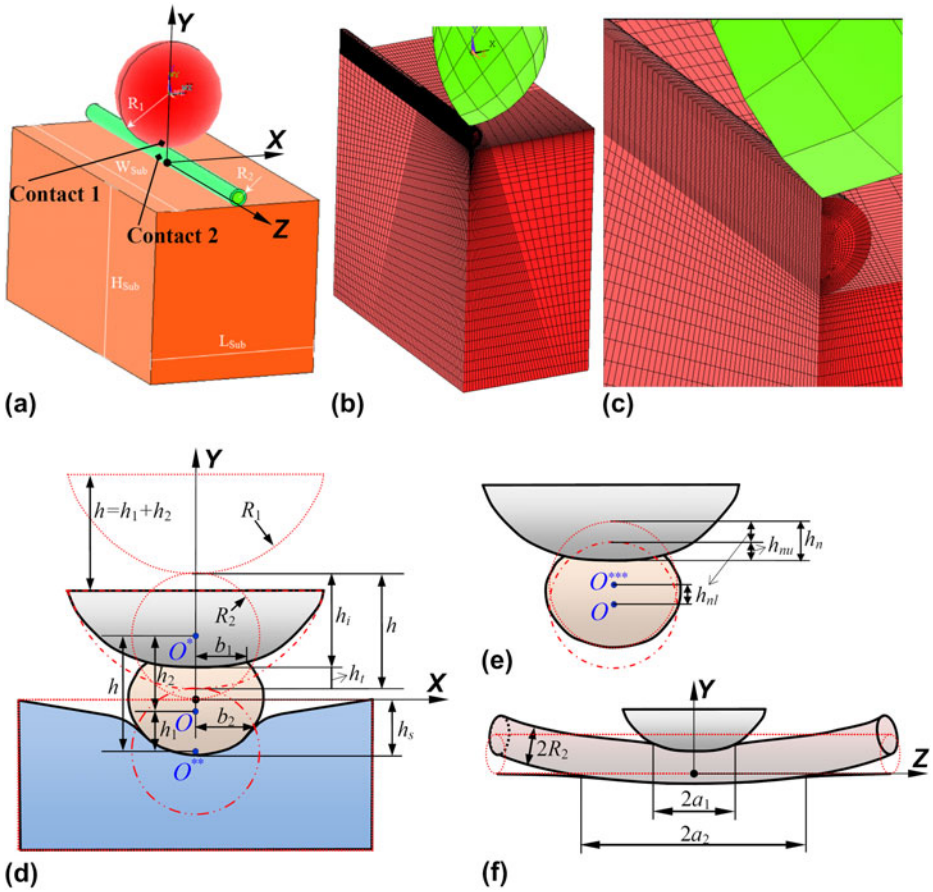


FIG. 1. A model of a lateral nanowire indentation. (a) The geometry, the coordinate system, and the associated parameters. (b) The FEA model. (c) A magnification of (b). (d)–(f) The schematics of a physical picture of nanowire indentation. In (d)–(f), the solid shapes are in the deformed configuration, and the dotted shapes are in the undeformed configuration. (d) A schematic at the X–Y plane, where the dash-dot shape is an undeformed indenter shape with its top overlapping with the top of the indenter in the deformed configuration, and the dash-double-dot circle is an undeformed nanowire shape (centered at O^{**}) with its top touching the undeformed indenter shape (the dash-dot shape). Here, O is the mass-center of the deformed nanowire, and O^{*} is the nanowire center in the undeformed configuration. (e) A partial replot of (d), where two undeformed nanowire shapes are also drawn: (i) a dash-dot circle centered at O, and (ii) a dotted circle (centered at O^{***}) with its bottom overlapping with the bottom of the deformed nanowire. (f) A schematic at the Y–Z plane. In schematics (d)–(f), a deformable indenter is assumed for generality, and the shapes are not in scale.

probing are supposed to be suitable for purely elastic contact, so that in the study, isotropic elasticity is assumed with $E_{GaN} = 301$ GPa, $\nu_{GaN} = 0.26$, $E_{Si} = 162$ GPa, and $\nu_{Si} = 0.22$.[9] Here, E represents Young's modulus, and ν represents Poisson's ratio.

A spherical indenter is assumed to be rigid for simplicity with a radius of $R_1 = 200$ nm. The nanowire radius $R_2 = 33$ nm. The nanowire length ($40R_2$) and the substrate dimensions ($20R_2 \times 20R_2 \times 40R_2$) are taken much larger than R_2. The indenter/nanowire and nanowire/substrate contacts will be referred as contacts 1 and 2, respectively. Only one quarter of the set up in Fig. 1(a) is modeled due to the symmetry. Contacts 1 and 2 are modeled as surface-to-surface contacts.[21] Contact 1 is frictionless. To study the adhesion effect, two limiting cases at contact 2 are modeled: (i) frictionless and freely separable, referred as the receding case, and (ii) bonded along the line initially in contact and frictionless elsewhere, referred as the bonded case. Figures 1(b) and 1(c) show the mesh used in the FEA model. A further mesh refinement with half mesh size results in a less than 5% difference in the indentation load P, indicating a good mesh convergence.

III. QUANTITATIVE PHYSICAL PICTURE

The quantitative physical picture of lateral probing of a nanowire should be first understood to provide quantitative analysis, which, however, has never been done adequately in the literature.[8–18] Figures 1(d)–1(f) illustrate a physical picture, showing various parameters including b_1 and b_2, the minor radii of contacts 1 and 2, respectively; a_1 and a_2, the major radii of contacts 1 and 2, respectively; h, the indentation depth; h_i, the displacement of the initial

https://doi.org/10.1557/jmr.2011.420 Published online by Cambridge University Press

contact point; h_t, the indenter-tip deformation ($h_t = 0$ for a rigid indenter); h_s, the substrate deformation; h_n, the nanowire deformation (the nanowire top-to-bottom relative displacement); h_{nu}, the nanowire upper-part deformation; and h_{nl}, the nanowire lower-part deformation. The upper and lower parts of the nanowire may be divided by its mass-center O. According to Figs. 1(d) and 1(e),

$$h = h_t + h_i = h_t + [h_n + h_s] = h_t + [(h_{nu} + h_{nl}) + h_s] \quad . \tag{1}$$

The contact deformation of contact 1, referred as h_1, may be estimated by summing the tip deformation h_t and the nanowire upper-part deformation h_{nu}, i.e.,

$$h_1 \approx h_t + h_{nu} \quad . \tag{2}$$

Similarly, the contact deformation of contact 2, referred as h_2, may be estimated by summing the nanowire lower-part deformation h_{nl} and the substrate deformation h_s, i.e.,

$$h_2 \approx h_{nl} + h_s \quad . \tag{3}$$

Thus, according to Eqs. (1)–(3),

$$h \approx h_1 + h_2 \quad , \tag{4}$$

which is expected on the basis of the double-contact (two contacts in series) model.

In our FEA modeling, h is the controlling input, h_2 can be measured by the displacement of the nanowire mass-center [see Fig. 1(d)], and then $h_1 \approx h - h_2$ according to Eq. (4).

Although the physical picture as shown in Figs. 1(d)–1(f) is obvious, according to our best knowledge, the contact 2 deformation h_2 was completely ignored in all previous reports[8–18] on lateral nanowire/nanotube indentation except in the Feng study.[9] However, h_2 could be pronounced especially for a relatively compliant substrate. For example, $h_2 \approx 60\%h$ according to our FEA results [see Figs. 2(a) and 2(b)].

IV. RESULTS AND DISCUSSIONS

A. Calculation of the FEA-determined and analytical results

Figure 2(a) shows the Y-displacement (see Fig. 1 for the coordinate system) field for the receding case at $h = 12$ nm ($P = 49.8$ μN), indicating a significant nanowire receding. Figure 2(b) shows the Y-displacement field for the bonded case at $h = 12$ nm ($P = 53.6$ μN), indicating a nanowire/substrate bonding situation.

All parameters shown in Figs. 1(d) and 1(e) can be directly measured or calculated from the FEA simulations. On the other hand, according to the Feng model,[9] if we know the elastic constants as well as the radii of nanowire and indenter, the load P and the elastic contact stiffness S ($=dP/dh$ due to purely elastic FEA modeling) are necessary and sufficient for estimating the nanowire hardness H. Here, the stiffnesses for contacts 1 and 2 ($S_1 = dP/dh_1$ and $S_2 = dP/dh_2$) as well as the contact radii can be calculated as analytical intermediate results. Thus, by comparing the FEA-determined results and the intermediate and final results based on the analytical model, we can verify the basic assumptions as well as the validity of the analytical model.

Figures 3(a)–3(f) plot the FEA-determined and analytical results, where the analytical results are calculated from P and S according to the analytical solution in the Feng study.[9] Here, to achieve a better comparison, the coefficient β' in Eqs. (6) and (8) in the Feng study[9] is recalibrated to be 1.0 (not 2.87 in the original Feng solution[9]). Here, β' is a geometry coefficient for receding problems,[9] which depends almost only on the contact geometry, e.g., $\beta' = 1.0$ for any plane contacts and $\beta' = 1.3$ for any axisymmetric contacts. Feng et al.[9] originally estimated $\beta' = 2.87$ based on the solely available analytical report by Castillo and Barber[22] on the contact between a cylinder and a rigid half-space.[22] However, $\beta' = 2.87$ may not be good for a stiff cylinder on a compliant substrate, e.g., the GaN-wire/Si-substrate case in this study. Therefore, based on the relation between the FEA-determined a_1 and a_2, we recalibrate and find $\beta' = 1.0$, indeed interestingly matching the value for the receding plane contact, as expected for the nanowire/substrate contact along the nanowire-axis direction.

B. Analysis of the FEA-determined results

To have a clear discussion, in this section, we focus only on the FEA-determined results, and the comparison between the FEA-determined and analytical results are discussed in the next section.

In Figs. 3(a)–3(f), the FEA-determined results are shown as thin black solid lines (the receding case) and thin black dash-dot lines (the bonded case). The subscript indicates the contact (contacts 1 or 2) to which the quantity is related to.

Figures 3(a)–3(d) indicate that, for each FEA-determined parameter, there is only a tiny discrepancy between the receding and bonded cases, implying that the adhesion condition at contact 2 has a small effect. Figure 3(b) indicates $h_2/h > 10\%$ for $P > 0.1$ μN, where 0.1 μN is the resolution of most commercial nanoindenters; consequently, it is problematic to ignore h_2, especially for compliant substrates, as in some previous studies.[11,16]

Figure 3(c) shows the stiffnesses, indicating that S_1 quickly increases with increasing P, whereas the increase of S_2 is not as significant; if $P > 5$ μN, $S_1 > S_2$, i.e., contact 2

https://doi.org/10.1557/jmr.2011.420 Published online by Cambridge University Press

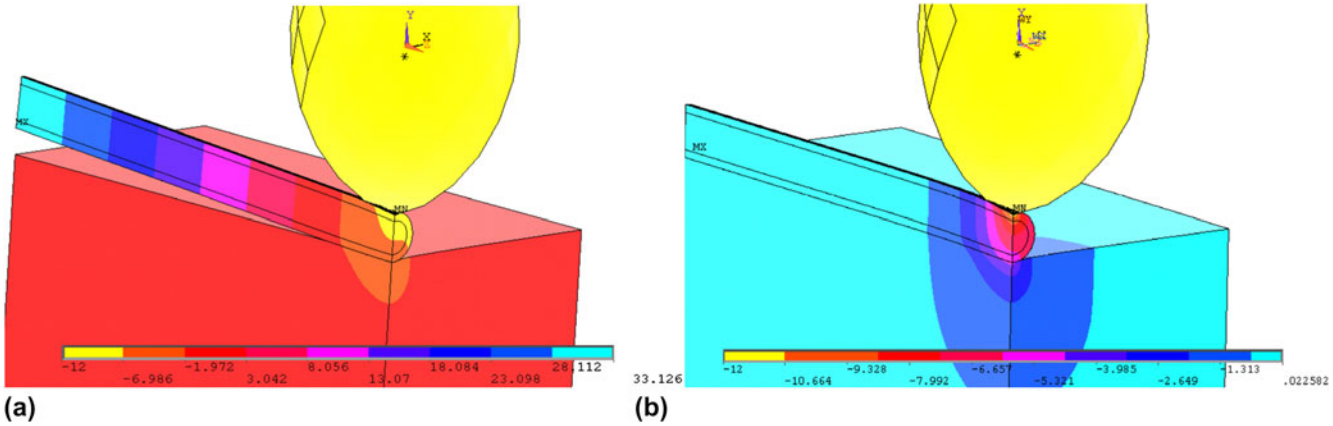


FIG. 2. The finite element analysis (FEA)-determined *Y*-displacement fields in the deformed configuration at $h = 12$ nm. (a) The receding case. (b) The bonded case.

is more compliant, and again we cannot ignore contact 2. Moreover, S_2 jumps to about 4 kN/m at $P = 0.1$ μN in both the receding and bonded cases as expected for a receding-like contact 2.[9] Furthermore, the overall stiffness S is less than S_1 and S_2, as expected for the double contacts in series.

Figure 3(d) shows the contact radii, where a_2 in the bonded case is determined by the position at which the stress σ_{YY} changes sign.[9] Figure 3(d) shows that for $P > 10$ μN, a_2 keeps constant in both the receding and bonded cases, implying that contact 2 is receding-like along the nanowire-axis direction.[9,22] Figure 3(f) shows the mean pressures calculated by $H \approx P/\pi ab$, indicating $H_1 > H_2$ as expected. It is surprising to see that even for a purely elastic contact 1, H_1 reaches a plateau for $P > 10$ μN, which may be due to the stress relaxation from the traction-free surface of the nanowire.[23]

C. Comparison of the FEA-determined and analytical results

In the following, we want to compare the FEA and analytical (the thick red lines) results. Here, the analytical results are calculated from the FEA-determined P and S according to the solution in the Feng study.[9]

In Fig. 3(d), because of the recalibration of β' as mentioned before, the analytical a_2 in the receding case matches well with the corresponding FEA result. It is surprising to see that the analytical a_2 in the bonded case also matches with the corresponding FEA result very nicely. However, in both the receding and bonded cases, Fig. 3(c) shows that the analytical solution largely underestimates S_1 but overestimates S_2, and Fig. 3(d) shows that the analytical solution largely underestimates a_1 and b_1, whereas Fig. 3(f) shows that the analytical solution largely overestimates the nanowire hardness H_1. The multifold reasons for these discrepancies are discussed in the following.

The dominant reason is that the contact-pressure distribution at contact 2 was assumed in the analytical model to be similar to a Hertzian distribution at an elliptical contact,[20] so that the Hertzian formula was used for estimating S_2,[9] i.e.,

$$S = 2\lambda E_r \sqrt{ab} \quad , \tag{5}$$

where E_r is the reduced modulus,[9] a and b are the major and minor radii, and λ is a parameter depending on b/a [see Eq. (2b) in the Feng study[9]]. To verify this reason, namely Eq. (5) is not good for contact 2, based on the FEA-determined a_2 and b_2, S_2 is calculated using Eq. (5) and plotted in Fig. 3(e) [see Eq. (5) in the legend] for the receding and bonded cases, indicating that Eq. (5) largely overestimates S_2.

This overestimation of S_2 by Eq. (5) is because the contact-pressure at contact 2 is too strongly concentrated to be described by a Hertzian distribution. To verify this strong stress concentration at contact 2, we may approximate contact 2 by an axisymmetric contact with its radius equal to the minor radius b_2, so that the Sneddon solution can be used for estimating S_2,[9,19,24] i.e.,

$$S = 2E_r b \quad , \tag{6}$$

where b is the contact radius of the circular contact.[24] Based on the FEA-determined b_2, the S_2 calculated using Eq. (6) is plotted in Fig. 3(e) (see "Sneddon, b_2" in the legend), indicating that the Sneddon solution estimates (slightly underestimates) S_2 fairly well, especially for large P. Therefore, the Sneddon solution based on the minor radius of contact 2 provides a good lower bound for estimating S_2.

Thus, in summary, these discrepancies between the FEA and analytical results due to the dominant reason can be explained as follows. When the Feng solution is used based on P and S, S_2 would be overestimated by Eq. (5), so S_1 would be underestimated due to $1/S = 1/S_1 + 1/S_2$ as shown in Fig. 3(c). Consequently, when we apply Eq. (5) to contact 1, namely $\sqrt{a_1 b_1} = S_1/(2\lambda_1 E_{r1})$,[9] to find out a_1 and b_1, they would be underestimated as shown in

https://doi.org/10.1557/jmr.2011.420 Published online by Cambridge University Press

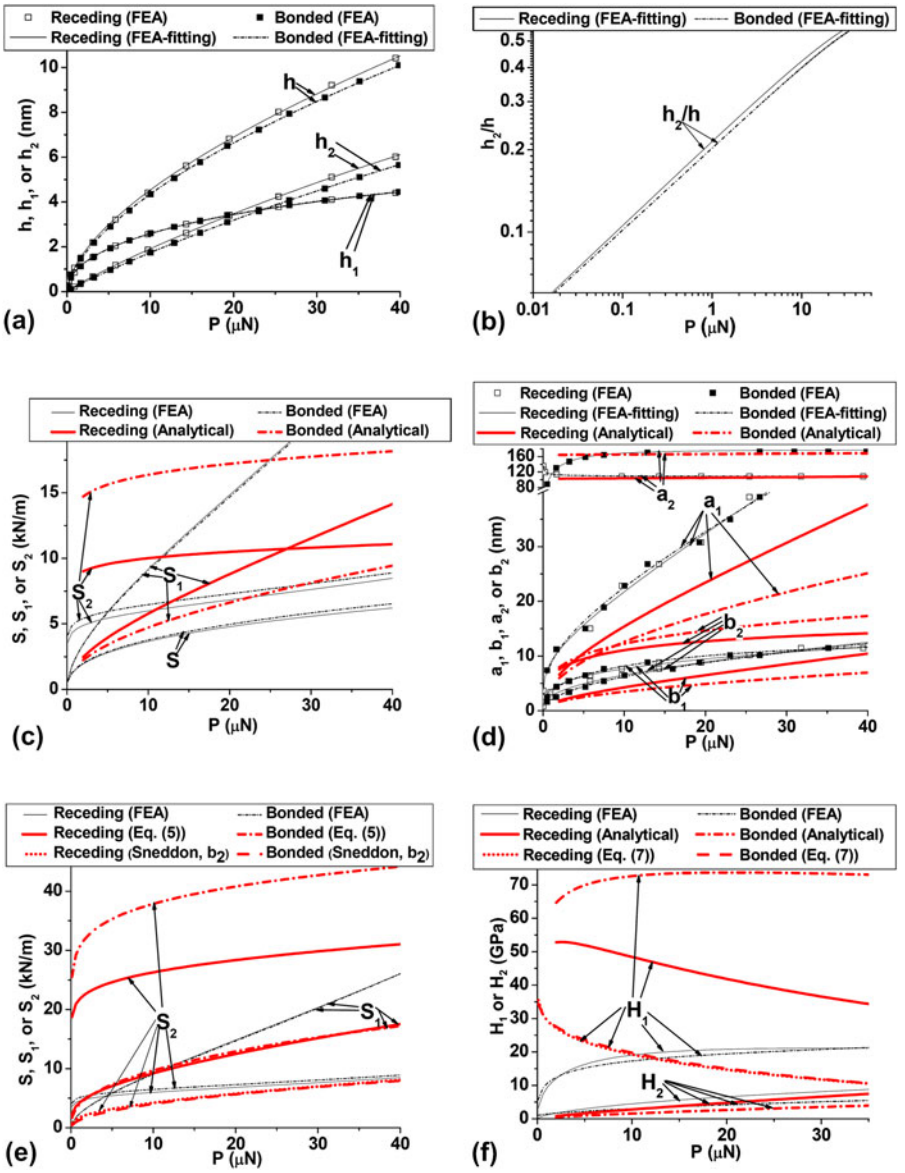


FIG. 3. The parameters plotted versus P, where the FEA results are black symbols or thin black lines, and the analytical results are thick red lines. Here, the thin lines are (or are based on) the fittings of the FEA results. (a) h, h_1, and h_2. (b) h_2/h. (c) S, S_1, and S_2. (d) a_1, a_2, b_1, and b_2. (e) S_1 and S_2, where the lines corresponding to "Sneddon, b_2" are virtually the same. (f) H_1 and H_2, where the lines corresponding to Eq. (7) are virtually the same.

Fig. 3(d) because of the underestimation of S_1. Therefore, H_1 ($\approx P/\pi a_1 b_1$) is overestimated, as shown in Fig. 3(f).

There is another discrepancy between the FEA and analytical H_1 results as shown in Fig. 3(f), namely, with increasing P, the FEA-determined H_1 increases, whereas the analytical H_1 decreases. The dominant reason for this discrepancy is that Eq. (5) is not good for contact 1 either, although Eq. (5) (the Hertzian elliptical contact equation) has been used for modeling nanowire and nanotube indentations in the Feng study and several other previous studies.[9,11,17] To verify this, based on the FEA-determined a_1 and b_1, S_1 can be calculated using Eq. (5) and plotted in Fig. 3(e) [see Eq. (5) in the legend] for the receding and bonded cases, indicating that the S_1 calculated by Eq. (5) does not match nicely with the FEA-determined S_1. This invalidity of Eq. (5) for contact 1 is due to the fact that Eq. (5) is derived based on small deformation,[20] i.e., $h_1 \ll R_2$ and $b_1 \ll R_2$, whereas $b_1/R_2 > 10\%$ for $P > 1$ μN as shown in Fig. 3(d), i.e., the small deformation condition is not satisfied.

In fact, noticing that $ab \approx S^2/\left(4\lambda^2 E_r^2\right)$ according to Eq. (5), we can estimate the contact pressure H for an Hertzian elliptical contact by

$$H = \frac{P}{\pi ab} = \frac{4P}{\pi S^2}\lambda^2 E_r^2 \quad . \tag{7}$$

https://doi.org/10.1557/jmr.2011.420 Published online by Cambridge University Press

To further verify that Eq. (5) is not good for contact 1, based on the FEA-determined S_1 and λ_1 (from the FEA-determined a_1 and b_1[9]), H_1 is calculated using Eq. (7) and plotted in Fig. 3(f) [see Eq. (7) in the legend], indicating that the H_1 calculated using Eq. (7) decreases with increasing P, and this decreasing trend is opposite to that of the FEA-determined H_1.

Therefore, we can conclude that Eq. (5) which is for Hertzian elliptical contact[20] cannot well describe contact 1, although the Hertzian contact theory has been widely used in the most advanced published models[9,11,17] for nanowire and nanotube indentations. As a future work, we would determine the upper limits of contact dimensions under which Hertzian elliptical contact theory can be applied and also provide a better theory (if analytically possible) being valid for large deformation.

V. CONCLUSIONS

In this study, to verify an analytical solution for lateral nanowire indentation, 3D FEA is performed on the basis of pure elasticity for a specific case: a spherical indention of a GaN nanowire on a Si substrate, showing significant deformation at contact 2 (the nanowire/substrate contact). Thus, it is problematic to ignore the deformation at contact 2, as in almost all previous studies. Moreover, the FEA modeling for the GaN-nanowire/Si-substrate case indicates that the adhesion condition at contact 2 (the nanowire/substrate contact) has a very small effect, and that contact 2 is receding-like along nanowire-axis direction. In addition, the mean pressure at contact 1 (the indenter/nanowire contact) reaches a plateau for large-enough indentation load.

Also, although the analytical solution can generally and qualitatively describe the FEA-determined results, there are discrepancies between the FEA and analytical results, which are mainly due to two reasons. The first reason is that the contact-pressure distribution at contact 2 is much more concentrated than that described by a Hertzian elliptical distribution. The second reason is that contact 1 cannot be well described by a Hertzian elliptical contact because of large contact deformation.

ACKNOWLEDGMENT

The authors acknowledge the financial support from a Keystone Innovation Starter Kit (KISK) grant from the Pennsylvania Department of Community and Economic Development.

REFERENCES

1. D.J. Sirbuly, A. Tao, M. Law, R. Fan, and P. Yang: Multifunctional nanowire evanescent wave optical sensors. *Adv. Mater.* **19**, 61 (2007).
2. Y.J. Choi, I.S. Hwang, J.G. Park, K.J. Choi, J.H. Park, and J.H. Lee: Novel fabrication of an SnO_2 nanowire gas sensor with high sensitivity. *Nanotechnology* **19**, 095508 (2008).
3. V.V. Dobrokhotov, M.M. Yazdanpanah, S. Pabba, A. Safir, and R.W. Cohn: Visual force sensing with flexible nanowire buckling springs. *Nanotechnology* **19**, 035502 (2008).
4. M.W. Li, R.B. Bhiladvala, T.J. Morrow, J.A. Sioss, K.K. Lew, J.M. Redwing, C.D. Keating, and T.S. Mayer: Bottom-up assembly of large-area nanowire resonator arrays. *Nat. Nanotechnol.* **3**, 88 (2008).
5. A.B.H. Tay and J.T.L. Thong: High-resolution nanowire atomic force microscope probe grown by a field-emission induced process. *Appl. Phys. Lett.* **84**, 5207 (2004).
6. S.P. Bao and S.C. Tjong: Mechanical behaviors of polypropylene/carbon nanotube nanocomposites: The effects of loading rate and temperature. *Mater. Sci. Eng., A* **485**, 508 (2008).
7. P.M. Ajayan, L.S. Schadler, and P.V. Braun: *Nanocomposite Science and Technology* (Wiley-VCH, Weinheim, 2003).
8. X.D. Li, P. Nardi, C.W. Baek, J.M. Kim, and Y.K. Kim: Direct nanomechanical machining of gold nanowires using a nanoindenter and an atomic force microscope. *J. Micromech. Microeng.* **15**, 551 (2005).
9. G. Feng, W.D. Nix, Y. Yoon, and C.J. Lee: A study of the mechanical properties of nanowires using nanoindentation. *J. Appl. Phys.* **99**, 074304 (2006).
10. X.D. Li, H.S. Gao, C.J. Murphy, and K.K. Caswell: Nanoindentation of silver nanowires. *Nano Lett.* **3**, 1495 (2003).
11. M.F. Yu, T. Kowalewski, and R.S. Ruoff: Investigation of the radial deformability of individual carbon nanotubes under controlled indentation force. *Phys. Rev. Lett.* **85**, 1456 (2000).
12. M. Minary-Jolandan and M.F. Yu: Reversible radial deformation up to the complete flattening of carbon nanotubes in nanoindentation. *J. Appl. Phys.* **103**, 073516 (2008).
13. H. Ni, X.D. Li, G.S. Cheng, and R. Klie: Elastic modulus of single-crystal GaN nanowires. *J. Mater. Res.* **21**, 2882 (2006).
14. T-H. Fang and W-J. Chang: Nanolithography and nanoindentation of tantalum-oxide nanowires and nanodots using scanning-probe microscopy. *Physica B* **352**, 190 (2004).
15. S.X. Mao, M. Zhao, and Z.L. Wang: Nanoscale mechanical behavior of individual semiconducting nanobelts. *Appl. Phys. Lett.* **83**, 993 (2003).
16. E.P.S. Tan and C.T. Lim: Nanoindentation study of nanofibers. *Appl. Phys. Lett.* **87**, 123106 (2005).
17. N. Lonnroth, C.L. Muhlstein, C. Pantano, and Y. Yue: Nanoindentation of glass wool fibers. *J. Non-Cryst. Solids* **354**, 3887 (2008).
18. H. Ni and X.D. Li: Young's modulus of ZnO nanobelts measured using atomic force microscopy and nanoindentation techniques. *Nanotechnology* **17**, 3591 (2006).
19. W.C. Oliver and G.M. Pharr: An improved technique for determining hardness and elastic-modulus using load and displacement sensing indentation experiments. *J. Mater. Res.* **7**, 1564 (1992).
20. K.L. Johnson: *Contact Mechanics* (Cambridge University Press, Cambridge, New York, 1987).
21. *Contact Technology Guide*, Vol. 12.1 (ANSYS, Inc., Canonsburg, PA, 2009).
22. J. Castillo and J.R. Barber: Lateral contact of slender prismatic bodies. *Proc. Math. Phys. Eng. Sci.* **453**, 2397 (1997).
23. Z.H. Xu and X.D. Li: Sample size effect on nanoindentation of micro-/nanostructures. *Acta Mater.* **54**, 1699 (2006).
24. G.M. Pharr, W.C. Oliver, and F.R. Brotzen: On the generality of the relationship among contact stiffness, contact area, and elastic-modulus during indentation. *J. Mater. Res.* **7**, 613 (1992).

https://doi.org/10.1557/jmr.2011.420 Published online by Cambridge University Press